DOI: 10.1002/smll.200800062

Multiscale Stochastic Simulations for Tensile Testing of Nanotube-Based Macroscopic Cables

Nicola M. Pugno, Federico Bosia, and Alberto Carpinteri*

Thousands of multiscale stochastic simulations are carried out in order to perform the first in-silico tensile tests of carbon nanotube (CNT)-based macroscopic cables with varying length. The longest treated cable is the space-elevator megacable but more realistic shorter cables are also considered in this bottom-up investigation. Different sizes, shapes, and concentrations of defects are simulated, resulting in cable macrostrengths not larger than ≈10 GPa, which is much smaller than the theoretical nanotube strength (≈100 GPa). No best-fit parameters are present in the multiscale simulations: the input at level 1 is directly estimated from nanotensile tests of CNTs, whereas its output is considered as the input for the level 2, and so on up to level 5, corresponding to the megacable. Thus, five hierarchical levels are used to span lengths from that of a single nanotube (≈100 nm) to that of the space-elevator megacable (≈100 Mm).

Keywords:
- carbon nanotubes
- elasticity
- fractures
- ruptures
- scaling

1. Introduction

Imagine a macroscopic bundle having the density, elastic modulus, and the mechanical strength of a single carbon nanotube (CNT). We could build fantastic structures such as a space-elevator megacable, perhaps the most intriguing concept in current materials science.

A space elevator[1] consists mainly of a very long cable attached to the Earth's surface and of the related climbers, similarly to a traditional elevator. If the cable is longer than ≈100 Mm, the centrifugal forces exceed the gravity of the cable, which will thus work under tension.[2] A space elevator would revolutionize the methodology for carrying payloads into space at low cost but its design is very challenging. The most critical component in the space-elevator design is undoubtedly the cable,[3,4] which requires a material with very high strength and low density. Considering carbon, the maximum stress reached at the geosynchronous orbit of the Earth is equal to ≈63 GPa. Only recently, after the discovery of nanotubes,[5] has such a large stress failure been experimentally measured in nanotensile tests of CNTs,[6–10] which are expected to have an ideal strength of ≈100 GPa. Note that for steel the maximum stress expected in the cable would be ≈383 GPa and for kevlar ≈70 GPa, both much higher than their strengths.[3] However, an optimized cable design can be achieved by considering a uniform tensile stress profile rather than a constant cross-sectional area.[2] Thus, at least theoretically, the cable could be built of any material by simply using a large enough taper ratio, that is, the ratio between the maximum cross-sectional area, at the geosynchronous orbit, and the minimum, at the Earth's surface. However, for steel or kevlar a giant and unrealistic taper ratio would be required, $\approx 10^{33}$ or $\approx 10^{8}$, respectively, whereas for defect-free CNTs the ratio would only need to be ≈2.[11] Nevertheless, such a value is expected to increase dramatically, as well as the cable mass, up to ≈613[4] for a carbon cable possessing a strength of ≈10 GPa. Such a lower strength, and thus the need for a larger taper ratio, emerges from our multiscale simulations, confirming independent deterministic and statistical results[3] that have recently suggested caution and, consequently, a dramatically modified design of the space-elevator cable[4] with respect to the current proposal.[12]

[*] Prof. N. M. Pugno, Prof. A. Carpinteri
Dept. of Structural Engineering and Geotechnics
Politecnico di Torino
Corso Duca degli Abruzzi 24, 10129, Torino (Italy)
Fax: (+39) 011-564-4899
E-mail: nicola.pugno@polito.it
Dr. F. Bosia
Dept. of Physics
Politecnico di Torino
Corso Duca degli Abruzzi 24, 10129, Torino (Italy)

WILEY InterScience® DISCOVER SOMETHING GREAT

© 2008 Wiley-VCH Verlag GmbH & Co. KGaA, Weinheim

Nonetheless, our multiscale strength predictions are evidently not only restricted to space-elevator megacables but are in general valid for nanotube-based macroscopic bundles. The new concept of ''superbridges'', that is, kilometer-long suspended bridges, based on nanotube cables, could be one example.

2. Hierarchical Multiscale Simulations

To numerically evaluate the strength of the space-elevator cable, the SE^3 code, formerly proposed by one of the authors,[3] is adopted. In previous studies,[3] preliminary simulations were carried out on a small piece of the space-elevator cable (basically our level 1 results), postponing a detailed and hierarchical investigation as the main topic of a subsequent, that is, the present, paper. Multiscale simulations are necessary in order to tackle the size scales involved, spanning over ≈15 orders of magnitude from nanotube length ($\approx 10^{-7}$ m) to space-elevator cable length ($\approx 10^{8}$ m), and also to provide useful information about cable scaling properties with length.

The cable is modeled as a N_{xk} by N_{yk} ensemble of subvolumes (or ''springs''), arranged in parallel sections, as shown in Figure 1. Each of the (primary) subvolumes is in turn constituted by $N_{x(k-1)}$ by $N_{y(k-1)}$ (secondary) subvolumes, arranged in parallel as before. This scheme is applied for k ''generations'', down to a level 1 subvolume, which comprises a N_{x1} by N_{y1} arrangement of ''springs'', or ''fibers'', representing the actual nanotubes (Figure 1). Here, we choose to adopt a scale-invariant approach, whereby the simulated structure appears the same at any given scale level (i.e., the length/width ratio is constant), and therefore choose $N_{x1} = N_{x2} = \ldots = N_{xk} = N_x$ and $N_{y1} = N_{y2} = \ldots = N_{yk} = N_y$. Overall, the cable comprises a total number of nanotubes given by $N_{tot} = (N_x\ N_y)^k$ and, in order to obtain the correct number in the space-elevator cable, which can be estimated as $N_{tot} \approx 10^{23}$,[3] we choose $k = 5$, $N_x = 40$ and $N_y = 1000$.

In silico hierarchical experiments have been carried out according to the following scheme:

a) Simulations at level 1:

- to the nanotubes (or fibers in the model) are assigned a fixed elastic modulus and a failure strength (nanoscale) Weibull statistical distribution, derived from observations on nanotensile tests of carbon nanotubes;[13]
- linearly increasing strains are applied to the fiber bundle, and at each code iteration the number of fractured fibers is computed (fracture occurs when local stress exceeds the nanotube failure strength) and the strains uniformly redistributed among the remaining intact fibers in each section (the uniform redistribution is plausible for independent nanotubes and in any case a stress concentration can be straightforwardly included in our model and would further reduce the failure stress);
- various quantities are monitored versus time during the simulation, for example, stress–strain, Young's modulus, number and location of fractured fibers, kinetic energy emitted, fracture energy absorbed, and so on. The simulation terminates when all fibers in one of the sections become fractured, separating the cable into two pieces.
- the above procedure is repeated numerous times in order to obtain reliable statistics for the various computed quantities, usually 10^3–10^4 times for each level.

b) Simulations at levels 2–5:

- the second-level fibers are those characterized in level 1 simulations, that is, their stiffness and strength distribution are derived from level 1 results. The same is true for level 3 simulations depending on level 2 results, and so on. This means that the elastic modulus and the statistical distribution of the failure stress of level i fibers are assigned according to those emerging from level $i-1$ simulations;
- again, repeated displacement-controlled virtual experiments are carried out at each level, with the same procedure as that outlined for level 1, leading hierarchically, at level 5, to results for the full-scale space elevator cable.

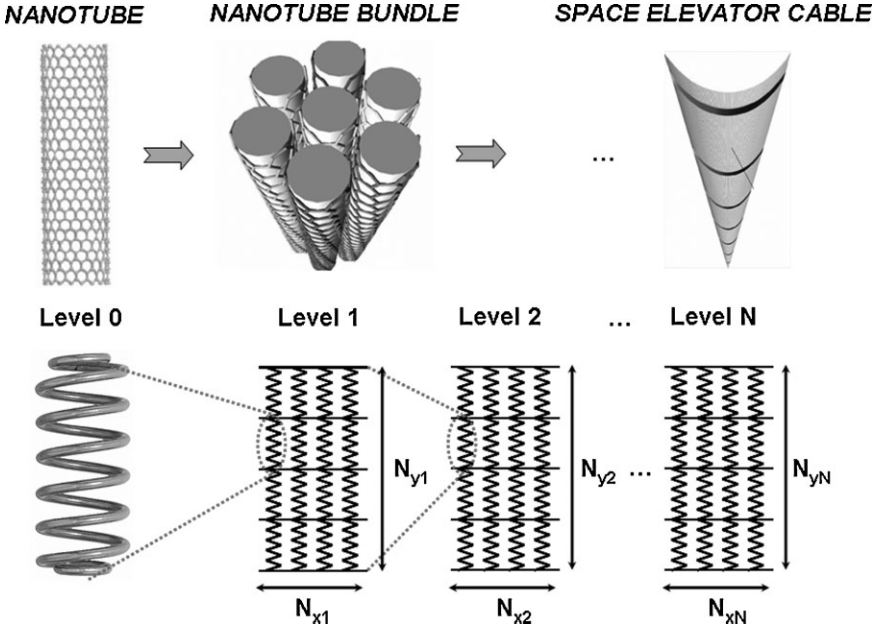

Figure 1. Schematic image of the adopted multiscale simulation procedure to determine the space elevator cable strength. Here, $k = 5$, $N_{x1} = N_{x2} = \ldots N_{x5} = 40$ and $N_{y1} = N_{y2} = \ldots N_{y5} = 1000$, so that the total number of nanotubes in the space elevator cable is $N_{tot} = (1000 \times 40)^5 \approx 10^{23}$.

3. ''Defect-Free'' Cables

The first simulation is carried out at nanotube level, that is, the fibers in the

 © 2008 Wiley-VCH Verlag GmbH & Co. KGaA, Weinheim

first-generation subvolume are $L_0 = 10^{-7}$ m in length, $w_0 = 10^{-9}$ m in width, their Young's modulus is $E_0 = 10^{12}$ Pa, and their strength σ_{f0} is randomly assigned, based on the nanoscale Weibull[13] distribution $P(\sigma_{f0}) = 1 - \exp[-(\sigma_{f0}/\sigma_0)^m]$ where P is the cumulative probability and the experimental values found for CNTs, $\sigma_0 = 34$ GPa, and $m = 2.7$.[13] This distribution accounts for statistical variations in the nanotube strength that are to be expected for various reasons, mainly the possible presence of defects in the nanotubes. However, the fiber bundle is considered to be "defective-free" at all levels, that is, no fibers are absent in the grid used in the simulations. The first-generation fiber bundle ($L_1 = 10^{-4}$ m in length) strength σ_{f1} is then derived, considering the experimental values of σ_{f0} and m for CNT, from a large number of repeated simulations (typically from 10^3 to 10^4), each with different randomly assigned local strengths, so as to build reliable statistics. The strengths of the fiber bundles at levels 2 to 5 (σ_{f2} to σ_{f5}), as explained above, are directly deduced from the numerically simulated distribution of strengths obtained at the previous level in each case. The strength σ_{f5} coincides with the final simulated space-elevator cable strength σ_f.

Results for the strength distributions $p(\sigma_{fi})$ at the various levels are shown by histograms in Figure 2. The level 1 distribution (Figure 2a) is centered around 15 GPa (as in the preliminary results reported by one of the authors[3]), is much narrower than the assumed distribution for the nanotube strengths, and can be adequately fitted with a Weibull distribution using $\sigma_0 = 13.14$ GPa and $m = 36.53$ as Weibull parameters (Figure 2a). The latter can be determined by introducing the variables $Y = \ln(-\ln(1-P))$ and $X = \ln\sigma$ and linearly fitting Y with respect to X, with the correlation coefficient of the fit taken as the evaluating parameter for the reliability of the fit. The fitting parameters allow the determination of σ_0 and m as $X = m^{-1}Y + \ln\sigma_0$. The simulations to determine the subvolume strength at level 2 are thus based on this distribution. Results of repeated simulations are shown in a typical histogram in Figure 2b. The distribution, which is the result of more than 10^4 repeated simulations, is again narrower than those at previous levels, and is centered around 11.13 GPa. In this case, some variation appears in the distribution form, with more than one peak appearing, and a Weibull function no longer correctly describes the dispersion of the data (continuous line in Figure 2b). To avoid this problem, the choice is made to use the actual distribution obtained in level 2 simulations (plotted by the histograms) as an input for level 3 simulations, that is, the strengths of the level 2 subvolumes constituting a level 3 subvolume are randomly selected from the distribution in Figure 2b. The same procedure is adopted in the simulations for levels 4 and 5, and results are shown in Figure 2c–e.

In each case, a decrease in the mean subvolume strength is noticed with respect to the previous level, with the main decrease occurring from level 1 to level 2 and a further decay in

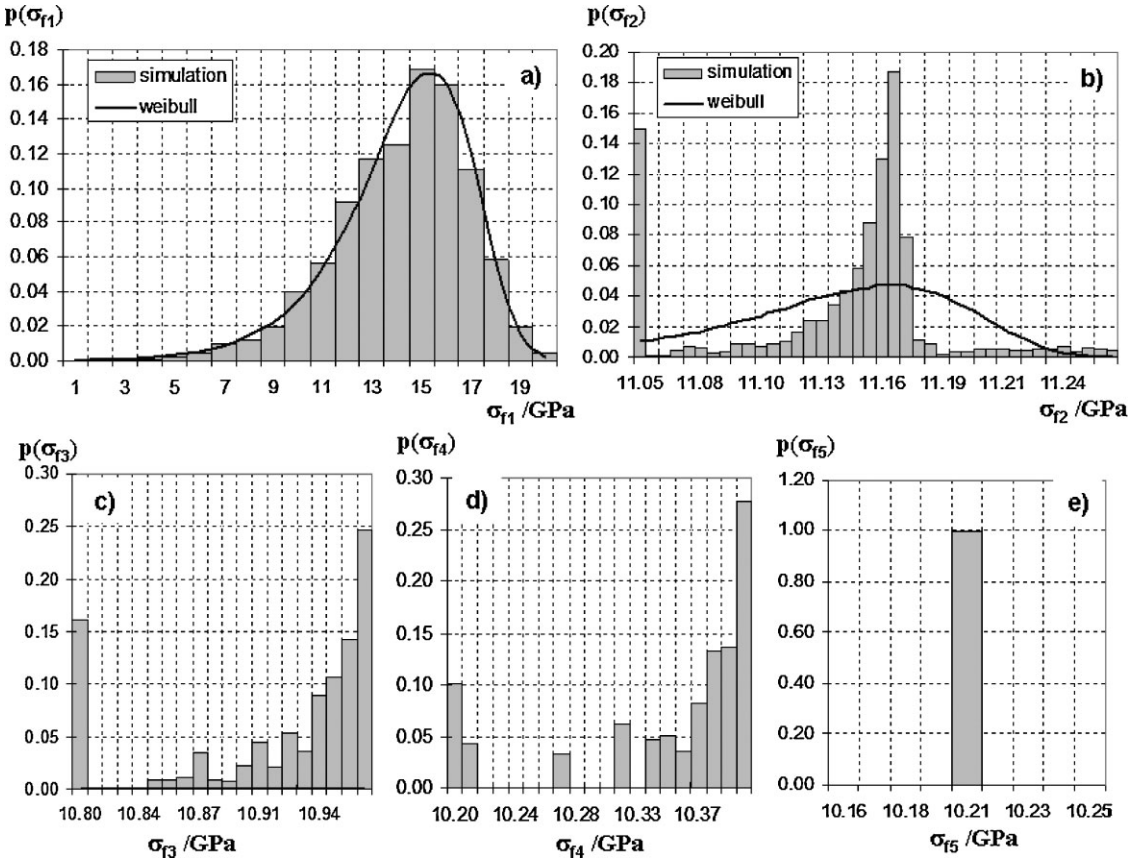

Figure 2. Simulation results for the subvolume strength distribution from level 1 to 5 (a to e, respectively). Only level 1 results can be adequately fitted with a Weibull distribution.

 © 2008 Wiley-VCH Verlag GmbH & Co. KGaA, Weinheim

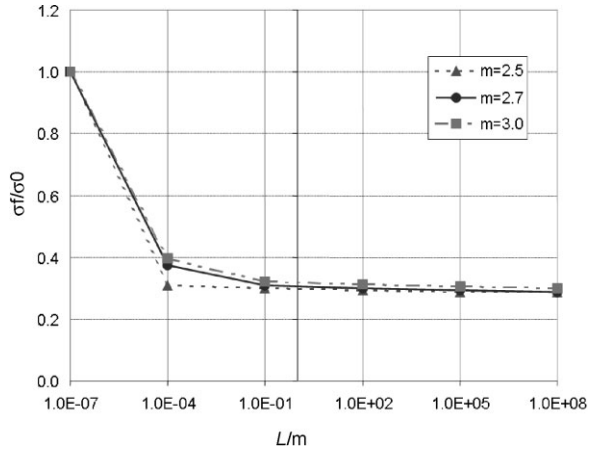

Figure 3. Results of simulations for the rescaled cable strength versus cable length using three different simulation parameters (m) in the assumed Weibull distribution.

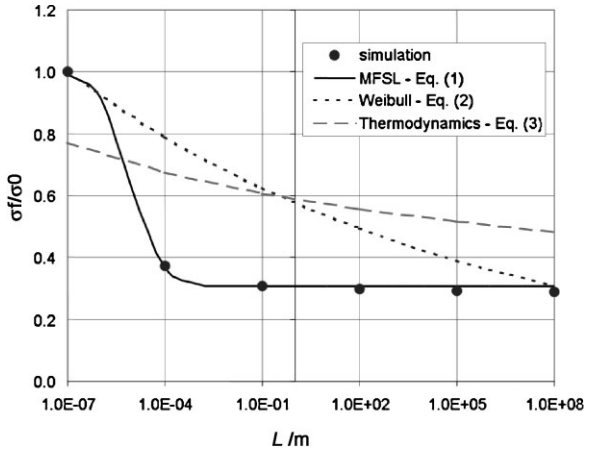

Figure 4. Comparison between simulations and analytical laws (see text) for the rescaled defect-free failure strength versus cable length.

the higher levels. Also, there is a decrease in the dispersion of results, with increasingly ''narrow'' distributions. The final space-elevator cable strength (level 5 simulation) can be evaluated at approximately 10.20 GPa, that is, less than 30% of the original mean nanotube strength and reduced to ≈10% of the theoretical nanotube strength. Results are plotted in Figure 3 for σ_f/σ_0 versus subvolume length L (indices are omitted for brevity). The ratio σ_f/σ_0 is considered in order to express results as fractions of the original nanotube strength σ_0. L is chosen as the relevant quantity to highlight the cable scaling properties and is plotted in logarithmic scale.

To evaluate the influence of the initial choice in the Weibull distribution at level 1, the same procedure as that described above has also been carried out for different plausible m values, in order to vary the distribution dispersion. Results are shown in Figure 3 for $m = 2.5$ and $m = 3.0$, together with those described previously for $m = 2.7$. It is evident that a smaller m slightly reduces the strengths, although to a negligible extent. The only significant difference is the more marked initial decrease in strength for $m = 3.0$, which remains in any case within 6% of the $m = 2.7$ value. The final elevator cable strengths differ in the three cases by 1% at most.

4. Scaling of Strength

Given the decay behavior of σ_f versus L obtained from simulations it is interesting to fit the data with simple analytical scaling laws. Various exist in the literature and one of the best known is the multifractal scaling law proposed by Carpinteri;[14] see also our related commentary.[15] The first law we wish to consider has recently been introduced:[16]

$$\frac{\sigma_f}{\sigma_{nano}} = \sqrt{\frac{\left(\frac{\sigma_{nano}}{\sigma_{mega}}\right)^2 - 1}{lS/V + 1} + 1} \tag{1}$$

where S and V are the surface and volume of the considered structure, respectively, σ_{nano} is its nanostrength, σ_{mega} is its megastrength, and l is a characteristic internal length. Note that for self-similar structures and for $\sigma_{nano} \gg \sigma_{mega}$ this law corresponds to the well-known Carpinteri scaling law. Here, we can choose σ_{nano} as the nanotube strength and σ_{mega} as the space-elevator cable strength obtained in simulations, that is, $\sigma_{nano} = 34$ GPa and $\sigma_{mega} = 10.20$ GPa. Also, $S/V = 1/L$, whereas l remains a free-fitting parameter. Results are shown in Figure 4 (''MFSL'' curve) for the various L considered at the different hierarchical levels ($m = 2.7$). The best fit is obtained for $l = 5 \times 10^{-5}$ m, where the analytical law is practically coincident with the simulated results. This can lead to an interpretation of l as a characteristic ''decay length'', in analogy with, for example, decay times in nuclear physics, beyond which the structure undergoes a considerable part of the strength reduction.

Another analytical scaling law for σ_f (''Weibull'' in Figure 4) can be obtained by considering the classical Weibull prediction:

$$\frac{\sigma_f}{\sigma_0} = kV^{-\frac{1}{m_1}} \tag{2}$$

where V is the volume of the structure, calculated here as the sum of the volumes of the 1.024×10^{23} nanotubes, and k and m_1 are fitting constants. Coincidence of σ_f/σ_0 with numerical results for $L = L_1$ and $L = L_5$ is obtained for $k = 0.29$ and $m_1 = 45$. However, the overall behavior does not match the numerical results, in that the initial decrease is not sharp enough.

An analytical law, representing the thermodynamical prediction of the upper bound of the strength, (''Thermodynamics'' in Figure 4, assuming the equality in Eq. (3)), is the following:[17]

$$\sigma_f \leq \frac{\sigma_{f_th}}{\sqrt{1 + \frac{k_b T \ln N}{E_C}}} \tag{3}$$

where $\sigma_{f_th} = 100$ GPa is the theoretical nanotube strength, $k_b = 1.38 \times 10^{-23}$ m^2 kgs^{-2} K^{-1} is the Boltzmann constant, T is the cable assembly temperature (≈4000 K), N is the number of

 © 2008 Wiley-VCH Verlag GmbH & Co. KGaA, Weinheim

carbon atoms in the cable ($\approx 10^6$ per nanotube), and $E_C = 7\ \text{eV} = 1.12 \times 10^{-18}\ \text{J}$ is the cohesive energy for carbon. In spite of the absence of any best-fit parameter, this analytical law captures the global simulated behavior, even if it underestimates the strengths for small L and overestimates them for large L.

5. Defective Cables

Next we wish to evaluate the influence of flaws or defects of various dimensions and at various levels on the cable structure, starting from the nanotube scale. This is done by introducing two types of void in the modeled fiber-bundle structure (i.e., setting the local stiffness and strength to zero):

a) randomly assigned, uniformly distributed, introduced alternatively at levels 1–4. Changing the simulation level at which voids are introduced amounts to considering the same defect concentrations but in different agglomerations (i.e., from evenly distributed, at level 1, to unevenly distributed, at level 4). This case is discussed in Section 5.1;
b) circular or elliptic in shape, distributed at random in the cable, introduced at level 1. This simulates the presence of medium-sized flaws or actual cracks in the structure, and is discussed in Section 5.2.

5.1. Randomly Distributed Defects

Three different defect volume percentages are considered, namely 10%, 50%, and 80%, introduced at various levels in the simulations. While the first of the three defect "concentrations" can be considered realistic for a structure such as the space-elevator cable, the second and third are included mainly for comparison purposes.

Results are shown in Figure 5, where the rescaled cable strengths versus length for the three different void percentages (defect 10%, defect 50%, defect 80%) are compared to those obtained for a defect-free ("intact") cable. The plots a–d illustrate results for voids introduced at levels 1, 2, 3, and 4 of simulations, respectively.

It is evident that the introduction of defects in increasing concentration induces an increasing reduction in cable strength that manifests itself starting from the level at which the voids are introduced. In the case of a void content of 10% the final elevator cable strength is reduced to 23% of the nanotube strength, with a further 24% reduction with respect to the nondefective cable. In the case of a void content of 50%, the final elevator cable strength is reduced to 7% of the nanotube strength, with a further 76% reduction with respect to the defect-free case. Finally, in the case of an 80% void content, the cable strength is reduced to 0 (percolation threshold).

To evaluate the effect of the level of defect "agglomeration" on the overall cable strength, one must plot the defective elevator cable strength versus the simulation level at which the void content is introduced. This is shown in Figure 6, for various cable lengths. From simulation results it would seem that the most significant effect on strength reduction, at a given void percentage, is obtained with an intermediate level of agglomeration, that is, when voids are introduced in the structure at an intermediate scale between the full length of the structure and the scale of its microstructure. Thus, for example, the strength reduction for the space elevator cable

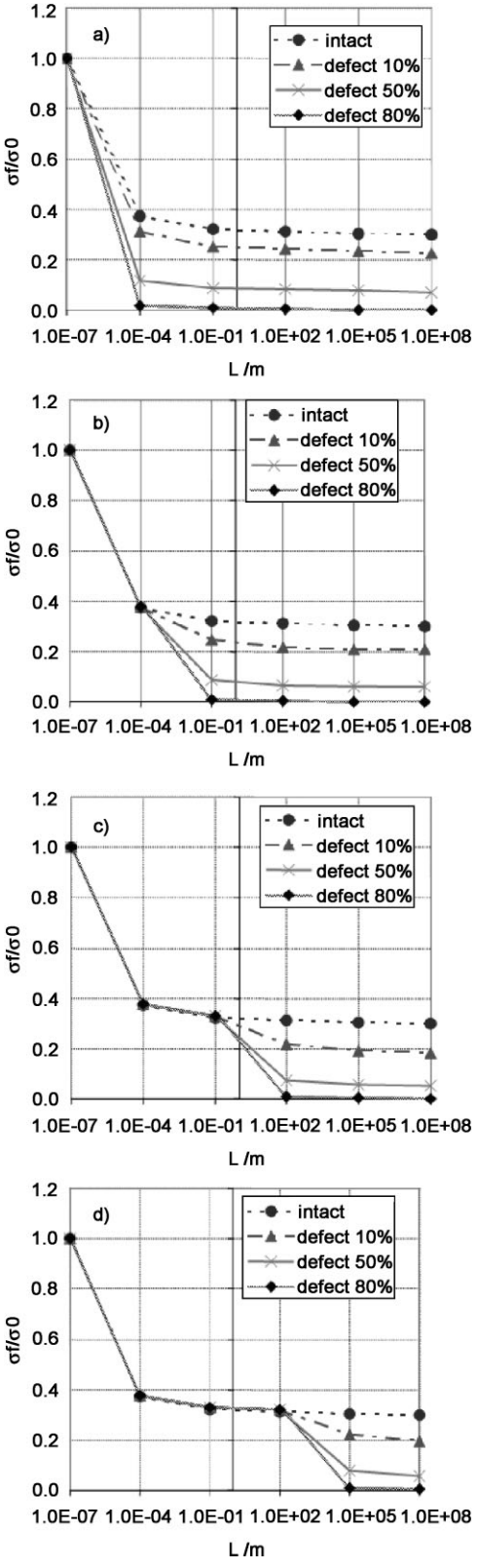

Figure 5. Rescaled defective cable failure strength versus cable length for various defect concentrations introduced at different levels (1-a, 2-b, 3-c, 4-d).

 © 2008 Wiley-VCH Verlag GmbH & Co. KGaA, Weinheim

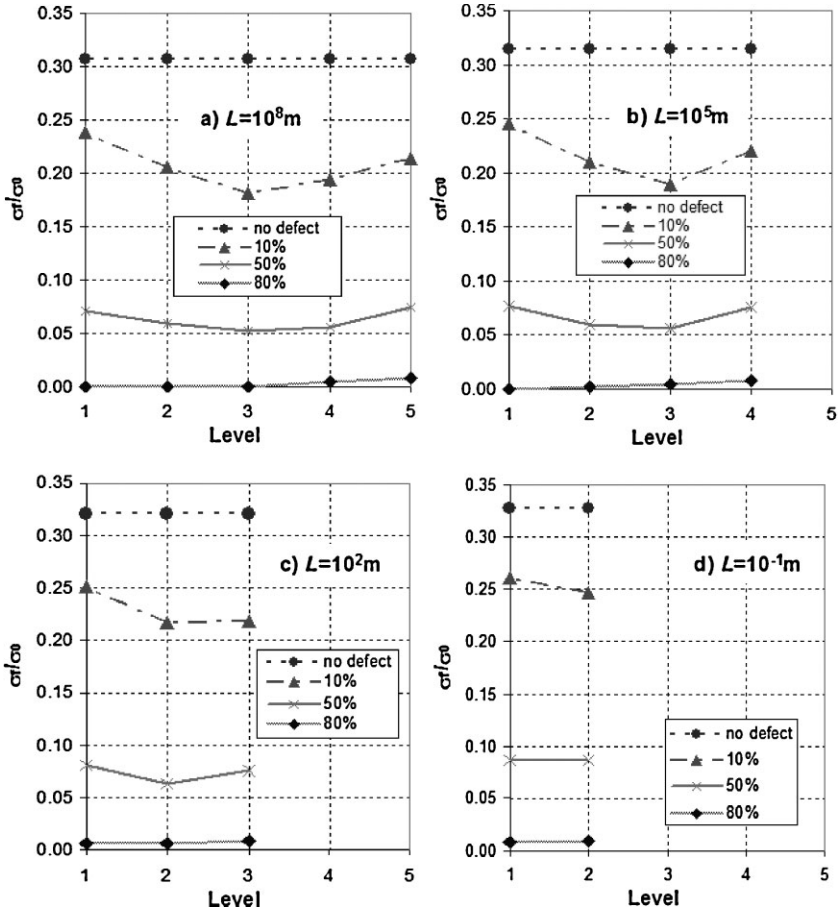

Figure 6. Rescaled defective failure strength versus level at which random defects are introduced for various cable lengths.

(Figure 6a, $L = 10^8$ m) is more consistent if defects are present at level 3, that is, on the 10^2 m scale. One possible explanation for this behavior is that it is the combination of two effects: on the one hand, the cable strength decreases with increasing void agglomeration; on the other hand, from a certain point onwards voids become increasingly sparse because of the fixed concentration, thus leading to a decrease in the strength reduction with size defect.

5.2. Circular or Elliptical Defects

The role of defects on the strength of the space-elevator cable is becoming a major concern, as detailed in Reference [3] (see an example of a damaged ribbon in Figure 7, from the space-elevator website[18]). To evaluate through simulations the effect of this type of defect, that is, holes of circular or elliptical shape, simulations are carried out in a manner similar to those described in the previous section, by setting the stiffness to zero in appropriate locations in the model structure. For simplicity, the defects are introduced at level 1 in all cases, and the following geometries are considered:

a) circular defect having a width of $1/10^{th}$ of the bundle width;
b) circular defect having a width of $1/4^{th}$ of the bundle width;

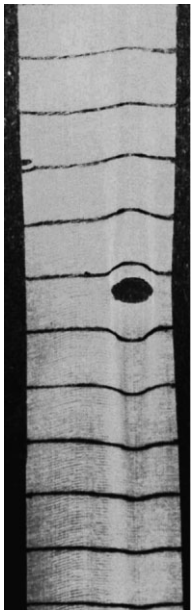

Figure 7. Elevator cable ribbon-type structure with a defect of non-negligible size, subjected to tension. [18]

 © 2008 Wiley-VCH Verlag GmbH & Co. KGaA, Weinheim

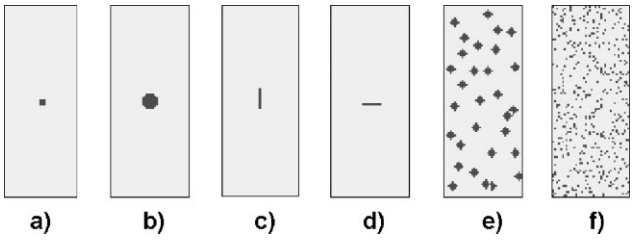

Figure 8. Defective cable configurations considered in simulations, illustrated on portions of the model specimen: a) circular defect having a width of $1/10^{th}$ of the specimen width; b) circular defect having a width of $1/4^{th}$ of the specimen width; c) vertical elliptical defect (crack parallel to the loading direction); d) horizontal elliptical defect (crack perpendicular to the loading direction); e) distributed circular defects giving a total void concentration of 10%; f) distributed point defects giving a total void concentration of 10%.

c) vertical elliptical defect (i.e., a crack parallel to the loading direction) and the same number of voids in the structure as case (a);
d) horizontal elliptical defect (i.e., a crack perpendicular to the loading direction) and the same number of voids in the structure as case (a);
e) randomly distributed circular defects of type (a), giving a total void concentration of 10%;
f) randomly distributed point defects giving a total void concentration of 10%, such as those considered in Section 5.1.

The considered structures are shown schematically in Figure 8.

Results for all the considered cases are shown in Figure 9 using a log scale for σ_f/σ_0 values in order to highlight the differences. It is apparent that the strength is only slightly reduced with respect to a nondefective cable when introducing a single circular defect with negligible size with respect to specimen width (simulation a). This is due to the aforementioned fact that the effect of small reticular imperfections is already accounted for when introducing a Weibull-distributed nanotube strength; therefore the actual circular defects do not influence results in a significant manner. The effect is more noticeable when introducing a single circular defect of greater size (simulation b). The shape of the defect plays a role, as simulations (c) and (d) show, in that defects simulating a crack placed transversally to the loading direction tend to reduce specimen strength in a more significant manner than those situated in a parallel direction, as expected. Finally, comparison of results from simulations (e) and (f) confirms the conclusion that a greater clustering of voids contributes to a further reduction in the strength of the cable, as seen in Section 5.1.

This effect is well known in the literature[19–21] and can be explained by the fact that voids of non-negligible size can introduce significant stress concentrations in the structure. This effect can be visualized in the simulations by fracture "maps" taken at progressive time intervals, highlighting how cracks evolve spatially in time. One such example is reported in Figure 10, which is a typical example of how damage propagates when a single circular defect is initially present in the cable.

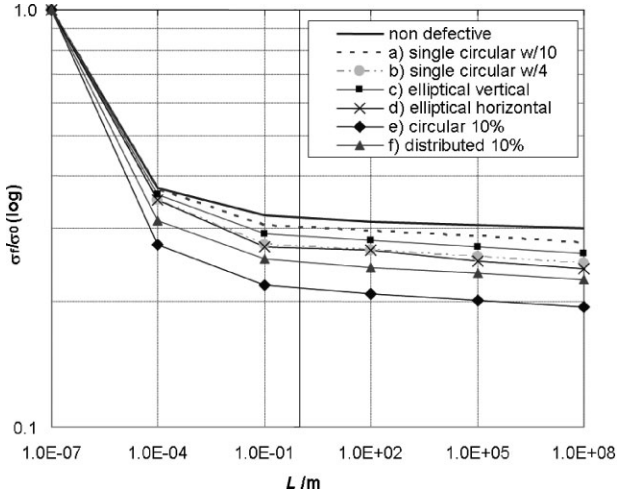

Figure 9. Rescaled defective cable failure strength versus length for various cases (see text and Figure 8).

6. Stiffness Reduction for Defective Cables

When addressing the effects of the presence of defects at various levels in the space-elevator cable, it is also of primary importance to evaluate the effects on cable stiffness.[22] The latter would have to be considered when evaluating, for example, the cable deformation, critical for the space-elevator stability.[23] Using the hierarchical approach outlined above, the cable stress–strain behavior is therefore calculated in simulations, as well as its stiffness reduction due to the

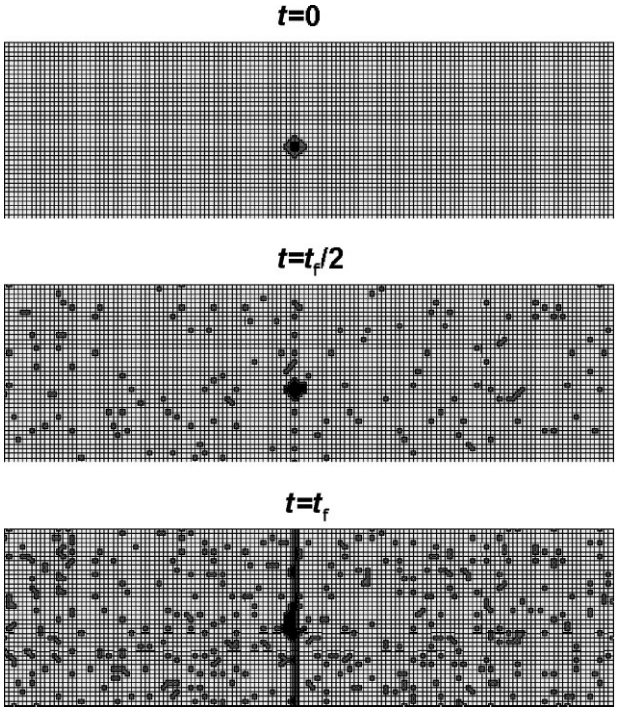

Figure 10. Fracture maps for an initially defective fiber bundle subjected to uniaxial traction at three successive time intervals; t_f is the time at which global failure occurs.

© 2008 Wiley-VCH Verlag GmbH & Co. KGaA, Weinheim

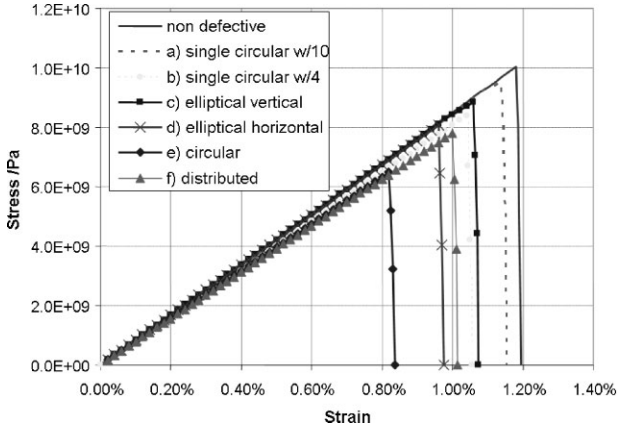

Figure 11. Cable stress–strain curves for various cases (see text and Figure 8).

presence of various types of defects. The stress–strain curves are shown in Figure 11. It is clear that the presence of defects affects these curves principally in their ultimate strain values, although some variation in the stiffness is visible (detailed calculations will be reported in a future paper). Ultimate strains vary from 0.84% to 1.2% depending on the type of defect considered, showing that this parameter is indeed of considerable relevance. All curves display brittle failure, as is to be expected from the type of strength distribution obtained numerically at this level (Figure 2e).

Results for the cable stiffness reduction due to the various types of defect are shown in Figure 12. As mentioned above, the decrease in cable stiffness is not as consistent as that of the cable strength but is nonetheless non-negligible, with a 15% overall reduction in the case of a defect-free cable (in the sense outlined in Section 1), which increases to a 22% reduction in the case of a randomly distributed 10% void content. Results for a cable with a single circular defect having a width of 1/10 of specimen differ only slightly from those for a nondefective cable, as do those for similarly sized single elliptical defects. Also, in this case the effect of defect clustering is less pronounced, for example, the stiffness reduction in the case of clustered defects (with a 10% concentration) is virtually the same as that of randomly distributed defects.

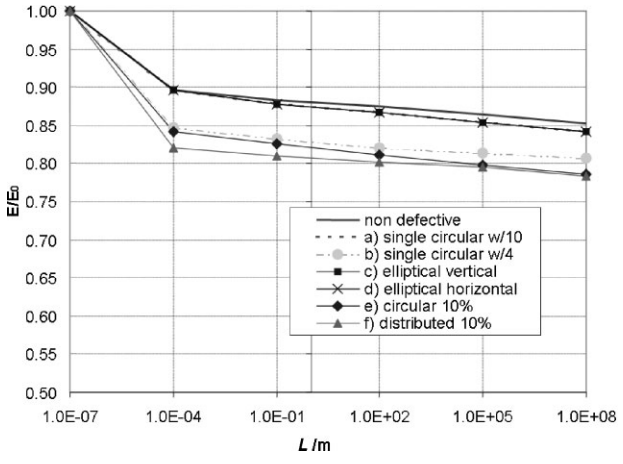

Figure 12. Rescaled defective cable stiffness versus length for various cases (see text and Figure 8).

7. Conclusions and Outlook

We have presented results deduced from thousands of multiscale stochastic simulations by using the SE^3 code[3] in order to perform the first in silico tensile tests of CNT-based macroscopic (up to mega) cables. Stress–strain curves, Young's modulus, number and location of fractured fibers, kinetic energy emitted, fracture energy absorbed, and so on, can be computed, in addition to the cable failure stress. Different sizes, shapes, and concentrations of defects are simulated, resulting in cable strengths of the order of ≈10 GPa. Regarding the concept of the space-elevator cable, this implies that the megacable strength is predicted to be much smaller than the theoretical nanotube strength (≈100 GPa), erroneously assumed previously in the space-elevator design.[12] Accordingly, the multiscale simulations suggest a taper ratio larger than ≈613, in spite of the current naïve proposal of 1.9. These results strongly confirm the previous and independent deterministic or statistical theoretical predictions[3,4,17] on the dramatic role expected to be played by even small defects in the megacable. Our predictions are conservative, since we have assumed perfect junctions between the nanotubes; the junctions are expected to be the weakest links,[24] even if advanced nanotechnology could lead to nearly perfect interconnects (i.e., junctions with a strength that is larger than that of the nanotubes themselves).

Our multiscale strength predictions are evidently not restricted only to space-elevator megacables but are in general valid for nanotube-based macroscopic bundles. For example, the new concept of ''superbridges'', that is, kilometer-long suspended bridges based on nanotube cables, could become technologically feasible in the near future.

Acknowledgements

N.P. and A.C. are supported by the ''Bando Ricerca Scientifica Piemonte 2006''–BIADS: Novel biomaterials for intra-operative adjustable devices for fine tuning of prostheses shape and performance in surgery. N.P. thanks Harry Kroto for commenting on the manuscript.

[1] Y. Artsutanov, V. Kosmos na Elektrovoze, Komsomolskaya Pravda, July 31 (**1960**); contents described in Lvov, V., *Science* **1967**, *158*, 946–947.
[2] J. Pearson, *Acta Astronautica* **1975**, *2*, 785–799.
[3] a) N. Pugno, *J. Phys.: Condens. Matter.* **2006**, *18*, S1971–1990; b) http://www.nature.com/news/2006/060522/full/news060522-1.html.
[4] N. Pugno, *Acta Materialia* **2007**, *55*, 5269–5279.
[5] S. Iijima, *Nature* **1991**, *354*, 56–58.
[6] M. F. Yu, B. S. Files, S. Arepalli, R. Ruoff, *Phys. Rev. Lett.* **2000**, *84*, 5552–5555.
[7] M. F. Yu, O. Lourie, M. J. Dyer, K. Moloni, T. F. Kelly, R. Ruoff, *Science* **2000**, *287*, 637–640.

 © 2008 Wiley-VCH Verlag GmbH & Co. KGaA, Weinheim

[8] A. H. Barber, I. Kaplan-Ashiri, S. R. Cohen, R. Tenne, H. D. Wagner, *Compos. Sci. Technol.* **2005**, *65*, 2380–2386.
[9] W. Ding, L. Calabri, K. M. Kohlhaas, X. Chen, D. A. Dikin, R. S. Ruoff, *Exp. Mech.* **2006**, *47*, 25–36.
[10] K. Koziol, J. Vilatela, A. Moisala, M. Motta, P. Cunniff, M. Sennett, A. Windle, *Science* **2007**, *318*, 1892–1895.
[11] B. C. Edwards, *Acta Astronautica* **2000**, *10*, 735–744.
[12] B. C. Edwards, E. A. Westling, *The Space Elevator: A Revolutionary Earth-to-Space Transportation System*, Spageo Inc., CA, **2003**.
[13] N. Pugno, R. Ruoff, *J. Appl. Phys.* **2006**, *99*, 024301.
[14] A. Carpinteri, *Int. J. Sol. Struct.* **1994**, *31*, 291–302.
[15] A. Carpinteri, N. Pugno, *Nat. Mater.* **2005**, *4*, 421–423.
[16] N. Pugno, *Acta Materialia* **2006**, *55*, 1947–1953.
[17] N. Pugno, *Nano Today* **2007**, *2*, 44–47.
[18] B. C. Edwards, The NIAC Space Elevator Program, from http://www.spaceelevator.com/
[19] N. Pugno, R. Ruoff, *Phil. Mag.* **2004**, *84*, 2829–2845.
[20] N. Pugno, *Int. J. Frac.* **2006**, *140*, 158–168.
[21] N. Pugno, *Int. J. Frac.* **2006**, *141*, 311–328.
[22] N. Pugno, *Appl. Phys. Lett.* **2007**, *90*, 043106.
[23] N. Pugno, H. Troger, A. Steindl, M. Schwarzbart, *Proc. of the 57th Int. Astronautical Congress*, October 2–6, **2007**, Valencia, Spain.
[24] F. M. Blighe, P. E. Lyons, S. De, W. J. Blau, J. N. Coleman, *Carbon* **2008**, *46*, 41–47.

Received: January 14, 2008
Revised: March 19, 2008

 © 2008 Wiley-VCH Verlag GmbH & Co. KGaA, Weinheim